Article ID: 1000-324X(2021)12-1330-07 **DOI:** 10.15541/jim20210063

Synthesis of Hierarchical Porous Nickel Phyllosilicate Microspheres as Efficient Adsorbents for Removal of Basic Fuchsin

WANG Tingting, SHI Shumei, LIU Chenyuan, ZHU Wancheng, ZHANG Heng

(School of Chemistry and Chemical Engineering, Qufu Normal University, Qufu 273165, China)

Abstract: Nickel phyllosilicates have shown considerable potential in many fields such as electrochemistry and catalysis owing to their specific structures, attracting a great attention on preparation and properties of them in recent years. In this study, $Ni_3Si_2O_5(OH)_4$ microspheres were synthesized *via* a hydrothermal method by using $NiCl_2$ and tetraethyl orthosilicate (TEOS) as the raw materials. Effects of Ni/Si molar ratio and alkali source on the phase composition, morphology and textural property of the products were investigated. Under optimized conditions, the as-synthesized $Ni_3Si_2O_5(OH)_4$ microspheres presented a nanosheets-assembled morphology with an average diameter of *ca*. 2.5 μm, S_{BET} of 119.6 $m^2 \cdot g^{-1}$, pore volume of 0.673 $cm^3 \cdot g^{-1}$, and Zeta potential measurements showed that they were negatively charged with pH ranging from 3 to 10. When employed as the adsorbents for basic fuchsin (BF), the $Ni_3Si_2O_5(OH)_4$ microspheres showed an adsorption capacity of 120.7 $mg \cdot g^{-1}$ with the removal efficiency up to 96.6% from 50 $mg \cdot L^{-1}$ solution, superior to most of the referred adsorbents in literatures, and the adsorption kinetic data can be well interpretated *via* the pseudo-second-order model. Data of the relationship between equilibrium adsorption capacity and BF concentration were well fitted by Freundlich isotherm model with the 1/*n* value of 0.1678, indicating that the surface was heterogeneous and the adsorption strength was strong.

Key words: nickel phyllosilicate; hydrothermal synthesis; dye removal; adsorption; basic fuchsin

As a big family of layered silicates, phyllosilicates include various natural clays, such as montmorillonite, saponite, laponite, attapulgite, and many synthetic metal phyllosilicates[1]. Because of their specific structural features and ion exchange properties, phyllosilicates have large application potential in the field of heterogeneous catalysis, electrocatalysis, waste water treatment, *etc*. In the past years, plenty of research works have been carried out by using natural clays as catalysts supports or adsorbents for dye removal after inorganic or organic modification[2-6]. In recent years, the synthesis and application of metal phyllosilicates, such as Ni[7-9], Co[10], Cu[11-12], Mg[13] containing phyllosilicates, have aroused more and more attention.

For nickel phyllosilicates, the difference in the ratio of tetrahedral and octahedral sheets generates two types of structures: (1∶1 and 2∶1 type nickel phyllosilicates) with the formula of $Ni_3Si_2O_5(OH)_4$ and $Ni_3Si_4O_{10}(OH)_2$[14-15]. The tetrahedral sheets consist of silicon-oxygen tetrahedra, which are linked by two-dimensional corner-sharing three of every four oxygen atoms so as to form sheets of indefinite extent, in which the ratio of silicon to oxygen is 2∶5. The octahedral sheets consist of two planes of closely packed O^{2-}, OH^- anions of octahedra with Ni^{2+} as the central cations. Based on this fundamental structure, nickel phyllosilicates can be assembled into different two-dimensional (2D) or three-dimensional (3D) architecture with enhanced application performances by using unique preparation methods. For instance, nanotubular $Ni_3Si_2O_5(OH)_4$ can be synthesized by hydrothermal methods in strongly alkaline environment and applied as lithium battery anode support materials[15-17]. Several efforts have been made to synthesize $Ni_3Si_2O_5(OH)_4$ with hollow sphere or core-shell structure by using SiO_2 microspheres as templates[18-19]. However, this preparation route often requires hard-controlled

Received date: 2021-02-01; **Revised date:** 2021-03-30; **Published online:** 2021-04-05
Foundation item: Natural Science Foundation of Shandong Province (ZR2018MB033); Undergraduate Training Program for Innovation and Entrepreneurship of Shandong Province (S201910446015)
Biography: WANG Tingting (1979–), female, Master. E-mail: wangting@qfnu.edu.cn
王婷婷(1979–), 女, 硕士. E-mail: wangting@qfnu.edu.cn
Corresponding author: ZHANG Heng, PhD, associate professor. E-mail: zhangheng@qfnu.edu.cn
张 恒, 博士, 副教授. E-mail: zhangheng@qfnu.edu.cn

conditions and subsequent complicated procedures for the removal of templates. Efficient preparation of $Ni_3Si_2O_5(OH)_4$ with 3D hierarchical structure is very meaningful for expanding its applications.

Nickel phyllosilicates have so far been well applied in the preparation of Ni-based catalysts. Considering their well-formed layered structure, nickel phyllosilicates are also expected to be very effective adsorbents for dye removal from waste water. However, to our best knowledge, no report focused on this issue is available up to now. In this study, $Ni_3Si_2O_5(OH)_4$ hierarchical porous microspheres were synthesized *via* a simple hydrothermal method using $NiCl_2$, tetraethoxysilane (TEOS) as the raw materials, and then were used as the adsorbent for the removal of basic fuchsin (BF) from simulated waste water.

1 Experimental

1.1 Synthesis of $Ni_3Si_2O_5(OH)_4$

All chemicals were analytical grade and obtained from Sinopharm Chemical Reagent Beijing Co., Ltd., Beijing, China. In a typical procedure for the synthesis of $Ni_3Si_2O_5(OH)_4$, 0.4420 g (2.12 mmol) TEOS and 64 mL deionized (DI) water were added to a conical flask, then 0.5043 g (2.12 mmol) $NiCl_2·6H_2O$ was added to the conical flask and dissolved completely. 0.8 g (13.3 mmol) urea was added to the solution followed by vigorous stirring for 0.5 h. The resultant solution was transferred to a Teflon-lined stainless steel autoclave with a capacity of 100 mL. The autoclave was sealed and heated to 210 ℃ and kept in an isothermal state for 12 h, then cooled down to room temperature. After washed with DI water, the solid product was collected and finally dried at 75 ℃ for 12 h.

1.2 Characterization

X-ray diffraction (XRD) patterns were recorded on a MiniFlex600 Powder X-ray powder diffractometer (Rigaku, Japan). Scanning electron microscopy (SEM) measurements were carried out on a JSM 6700F field emission scanning electron microscope (JEOL, Japan). Transmission electron microscopy (TEM) measurements were carried out on a JEM-2100PLUS high resolution transmission electron microscope (JEOL, Japan). Nitrogen adsorption-desorption isotherms were measured using a Kubo-X1000 surface area and porosity analyzer (Builder Electronic Technology, China), and the specific surface areas were calculated using the Brunauer-Emmett-Teller (BET) equation. Zeta potential of the sample was tested on a ZEN3700 Zeta potential analyzer (Malvern, UK).

1.3 Adsorption removal of BF

For a typical adsorption removal of BF from simulated waste water, 20 mg $Ni_3Si_2O_5(OH)_4$ microspheres were mixed with 50 mL basic fuchsin solution (original concentration: 50 $mg·L^{-1}$). At preset period, 2 mL suspension was taken from the solution, and the liquid was monitored by a UV756CRT UV-Vis spectroscope (Yoke Instrument, China) after solid-liquid separation. The adsorption capacity of the adsorbents for BF was evaluated by the following Eq. (1):

$$q_t = \frac{(c_0 - c_t)V}{m} \quad (1)$$

where q_t ($mg·g^{-1}$) is the adsorption capacity at time t, c_0 and c_t ($mg·L^{-1}$) the original and real-time concentrations of BF solution, respectively, V (L) is the volume of the employed BF solution , and m (g) is the mass of the employed adsorbent.

2 Results and discussion

2.1 Composition and morphology of $Ni_3Si_2O_5(OH)_4$ microspheres

$NiCl_2$ and TEOS were used as the raw materials to synthesize nickel silicates through the urea-assisted hydrothermal method. The effect of Ni/Si molar ratio on the phase composition of the products is shown in Fig. 1. In previous study it was found that the 2∶1 type nickel phyllosilicate $Ni_3Si_4O_{10}(OH)_2$ can be synthesized with a low Ni/Si molar ratio (0.25∶1)[20]. Fig. 1 shows that the 1∶1 type $Ni_3Si_2O_5(OH)_4$ is easier to form when the Ni/Si molar ratio is set up to or higher than 0.5∶1, and the diffraction peak at 2θ=12.2° which is associated with the (002) plane of $Ni_3Si_2O_5(OH)_4$, is obviously increased with the increase of Ni/Si molar ratio from 0.5∶1 to 1.5∶1. Besides this characteristic peak for the layered structure of $Ni_3Si_2O_5(OH)_4$, there is another small diffraction peak appearing at 2θ=8.3°, which represents a larger layer spacing (1.067 nm) than the layer spacing of $Ni_3Si_2O_5(OH)_4$ (0.0736 nm), but smaller than that of $Ni_3Si_4O_{10}(OH)_2$ (1.510 nm). It can be considered an intermediate state transforming from 2∶1 type to 1∶1 type layered structure. As shown in Fig. 1, single phase $Ni_3Si_2O_5(OH)_4$ was obtained with a Ni/Si molar ratio of 1∶1. And the further increase of Ni/Si molar ratio resulted in the formation of NiOOH (JCPDF 06-0141).

Fig. 2 shows the SEM and TEM images of the $Ni_3Si_2O_5(OH)_4$ hydrothermally synthesized with the Ni/Si molar ratio of 1∶1 in the raw materials. As shown in Fig. 2(a, b), the $Ni_3Si_2O_5(OH)_4$ microspheres present a microsphere-shaped morphology with an average diameter of *ca*. 2.5 μm. The magnified SEM image indicates

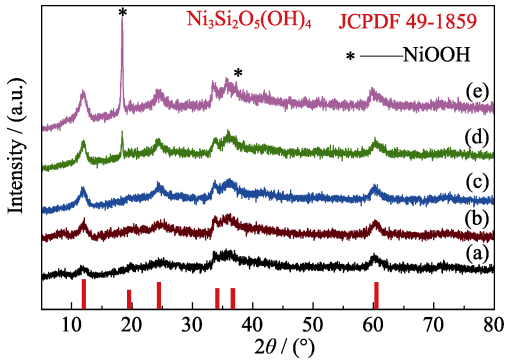

Fig. 1 Effect of Ni/Si molar ratio on the phase composition of the products hydrothermally synthesized at 210 ℃ for 12 h with different Ni/Si molar ratios

(a) 0.5 : 1; (b) 0.75 : 1; (c) 1 : 1; (d) 1.25 : 1; (e) 1.5 : 1

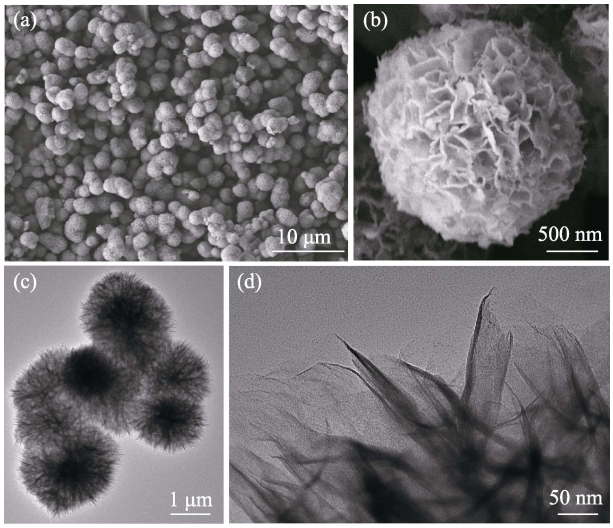

Fig. 2 SEM and TEM images of the $Ni_3Si_2O_5(OH)_4$ microspheres hydrothermally synthesized at 210 ℃ for 12 h with Ni/Si molar ratio of 1 : 1

that these microspheres are porous and assembled by nanosheets. TEM images further confirm that the porous microspheres are composed of nanosheets (Fig. 2(c, d)). In Fig. 2(d), layered structure can be found at the edge of the nanosheets, which corresponds to the (002) plane of $Ni_3Si_2O_5(OH)_4$.

2.2 Textural properties of $Ni_3Si_2O_5(OH)_4$ microspheres

The N_2 adsorption/desorption isotherms and the pore size distribution (PSD) curves of the hydrothermal products with different Ni/Si molar ratios in the raw materials are illustrated in Fig. 3 and Fig. 4, respectively. The experimental data for specific surface areas, porous volumes and the average pore sizes are summarized in Table S1. All of the samples exhibit similar adsorption-desorption isotherms which can be assigned to type IV adsorption isotherms with type H2 hysteresis loops, implying the presence of ink-bottle-like pores. As shown

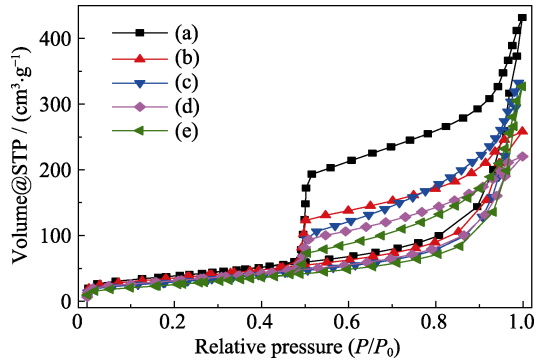

Fig. 3 N_2 adsorption-desorption isotherms of the products hydrothermally synthesized at 210 ℃ for 12 h with different Ni/Si molar ratios

(a) 0.5 : 1; (b) 0.75 : 1; (c) 1 : 1; (d) 1.25 : 1; (e) 1.5 : 1

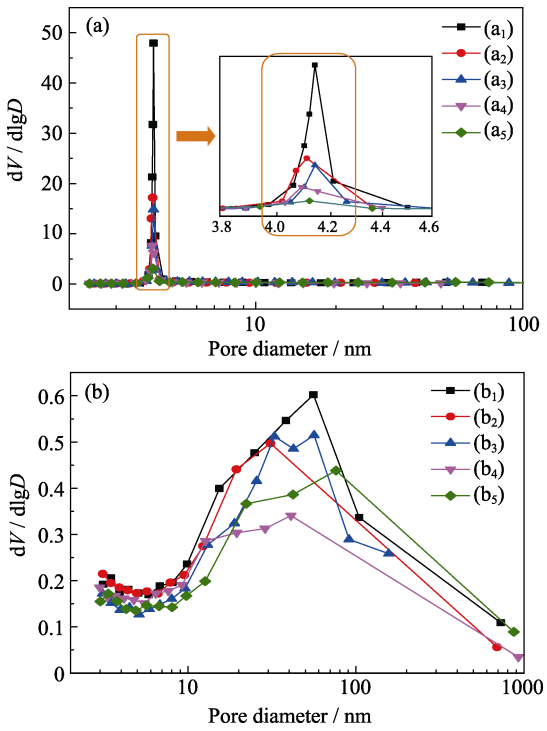

Fig. 4 Pore size distribution derived from desorption (a) and adsorption (b) branch of the isotherm of the products hydrothermally synthesized with different Ni/Si molar ratios

(a_1, b_1) 0.5 : 1; (a_2, b_2) 0.75 : 1; (a_3, b_3) 1 : 1; (a_4, b_4) 1.25 : 1; (a_5, b_5) 1.5 : 1

in Table S1, the BET surface areas were significantly affected by Ni/Si molar ratio in the raw materials. With the increase of Ni/Si ratio from 0.5 : 1 to 1.5 : 1, the BET surface areas decreased successively from 139.4 $m^2 \cdot g^{-1}$ to 95.5 $m^2 \cdot g^{-1}$.

For the materials with small mesopores (pore diameter 2–10 nm), the tensile strength effect (TSE) during the adsorption measurements could significantly affect the adsorption isotherm, and therefore leading to incorrect assessment of PSD when the BJH model was applied to the desorption branch of the isotherm. Instead, the adso-

rption branch is hardly affected by the TSE phenomenon and is preferred for pore size calculations as pointed out in the literature[21]. In this study, the desorption branch and the adsorption branch were both adopted to analyze the PSD as shown in Fig. 4. The desorption branch indicates that all products have dominant mesopores centered at about 4.1 nm, which is completely different as compared to the results obtained from the adsorption branch. This large difference should be attributed to the TSE phenomenon, which leads to the misinterpretation of the PSD derived from the desorption branch. In fact, the prominent peak observed around 4.1 nm is not the real porous property. Wide PSD, especially in the range from 20 to 100 nm, is observed for all products according to the adsorption branch. This is in good agreement with the SEM and TEM images, in which piled pores produced by the assembly of nanosheets can be found.

2.3 Effect of alkali source on the formation of $Ni_3Si_2O_5(OH)_4$ microspheres

To better understand the effect of urea on the formation of the $Ni_3Si_2O_5(OH)_4$ microspheres, various alkali source and different adding amount of urea were employed for the hydrothermal synthesis. XRD patterns and SEM images of the products are shown in Fig. 5. Without alkali addition, there was no solid product obtained after the hydrothermal reaction. The addition of ammonia, sodium hydroxide and urea can render the formation of $Ni_3Si_2O_5(OH)_4$. The reaction is considered as the following Eq. (2):

$$2(C_2H_5O)_4Si+3Ni^{2+}+6OH^-+3H_2O\rightarrow Ni_3Si_2O_5(OH)_4+8C_2H_5OH \quad (2)$$

Thus, alkaline condition is necessary for the formation of the product. Fig. 5 shows that the morphologies of the products vary dramatically with different alkali sources. When ammonia was used, the product was mainly composed of porous near-spherical particles with the diameter less than 1 μm. In comparison, the use of sodium hydroxide resulted in the formation of dense irregular blocks. It shows that mild alkali environment is conducive to the formation of porous structure. The presence of urea in the hydrothermal process can also provide mild alkali environment as the situation in ammonia, because its decomposition in aqueous solution leads to the release of CO_2 and NH_3 into the system. NH_3 can easily dissolve into water, generating NH_4^+ and OH^- ions. In this basic aqueous solution, TEOS reacts with Ni^{2+} and OH^- ions to form $Ni_3Si_2O_5(OH)_4$. Yet there are two differences compared with that using ammonia directly. Firstly, OH^- ions were gradually released with the decomposition of urea. It did not cause the rapid formation of abundant crystal nucleus, and larger particles would be gradually formed

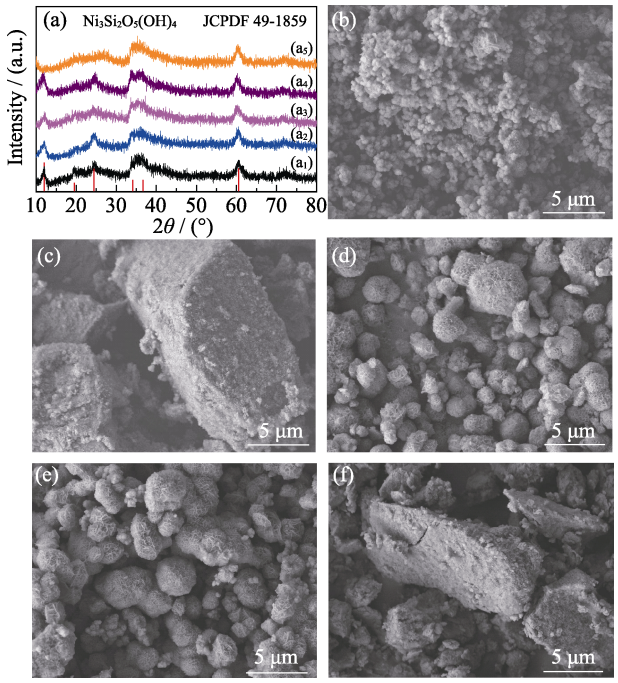

Fig. 5　Effect of alkali source on composition and morphology of the products

(a_1, b) Ammonia, 26.6 mmol; (a_2, c) Sodium hydroxide, 26.6 mmol; (a_3, d) Urea, 3.33 mmol; (a_4, e) Urea, 6.66 mmol; (a_5, f) Urea, 20.0 mmol

by the subsequent crystal growth. On the other hand, the presence of CO_2 bubbles in the solution can be heterogeneous nucleation centers according to the previous reports[22-23]. $Ni_3Si_2O_5(OH)_4$ tends to aggregate together around the CO_2 bubbles and self-assemble into larger particles, resulting in the porous structure of the final products. It was found that SiO_2 particles formed on the surface of the microspheres under the conditions of low temperature or short time hydrothermal treatment, as revealed in the synthesis of $Ni_3Si_4O_{10}(OH)_2$[20]. It is considered that besides the reaction shown in Eq. (2), base-catalyzed hydrolysis of TEOS takes place with the gradually decomposition of urea, leading to the formation of SiO_2. As the reaction approaches completion, the concentration of OH^- ions is thereby increased. Then the SiO_2 formed through the hydrolysis of TEOS is etched under this elevated alkaline condition. Based on the above analysis, the possible formation mechanism is illustrated in Fig. 6.

As shown in Fig. 5(f), the hydrothermal product turns to be dense irregular blocks with the amount of urea increasing to 20.0 mmol. Besides, its composition is different from the other samples. The disappearance of the diffraction peak at 2θ=12.2° can be detected in Fig. 5(a_5), and it obviously shifts to low diffraction angle. This sample is more likely composed of $Ni_3Si_4O_{10}(OH)_2$, indicating that excessive urea makes more TEOS participate in the reaction.

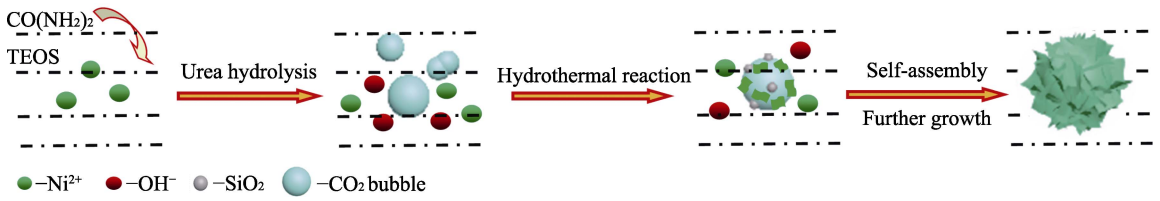

Fig. 6 Schematic illustration for the formation of $Ni_3Si_2O_5(OH)_4$ microspheres

2.4 Adsorption of BF on $Ni_3Si_2O_5(OH)_4$ microspheres

The as-synthesized $Ni_3Si_2O_5(OH)_4$ microspheres were applied as adsorbent for the removal of BF from simulated waste water. BF is a kind of cationic dye with the molecular structure as shown in Fig. 7(a). $Ni_3Si_2O_5(OH)_4$ microspheres are negatively charged according to the Zeta potential measurements as shown in Fig. 7(b). Thus, charge-charge interaction contribute to the adsorption of BF on $Ni_3Si_2O_5(OH)_4$ microspheres. At different pH, the variations of the adsorption rate and adsorption capacity as a function of contact time with the $Ni_3Si_2O_5(OH)_4$ microspheres dosage of 20 mg in a 50 $mg\cdot L^{-1}$ solution (50 mL) are displayed in Fig. 7(c). Obviously, the amount of adsorbed BF increased with the contact time increasing and then reached equilibrium. In the first 5 min, the removal efficiency ($(1-c_t/c_0)\times100\%$) was up to 63.2%, 69.0% and 76.8% at pH=4, 7 and 9, respectively, representing a quite rapid adsorption rate at the beginning of the contact between BF and the adsorbent. The increase of adsorption rate with the increase of pH can be attributed to the higher negative charge. After the first 5 min, the adsorption was significantly getting slow and gradually reached equilibrium. The ultimate adsorption capacity within 180 min was calculated to be 98.3, 120.7 and 111.5 $mg\cdot g^{-1}$ at pH=4, 7 and 9, respectively. The fast adsorption at the initial stage might cause pore structure block, resulted in the decrease of adsorption capacity at pH=9.

The adsorption performances of the samples with different Ni/Si molar ratios are shown in Fig. 7(d). As aforementioned, the product was composed of $Ni_3Si_4O_{10}(OH)_2$ when the Ni/Si molar ratio was 0.25 : 1, and its ultimate adsorption capacity within 180 min was 100.8 $mg\cdot g^{-1}$. With the increase of Ni/Si molar ratio, the adsorption capacity was greatly increased higher than 120 $mg\cdot g^{-1}$ for the samples (Ni/Si molar ratio of 0.5 and 0.75), which was a very similar performance as on the sample

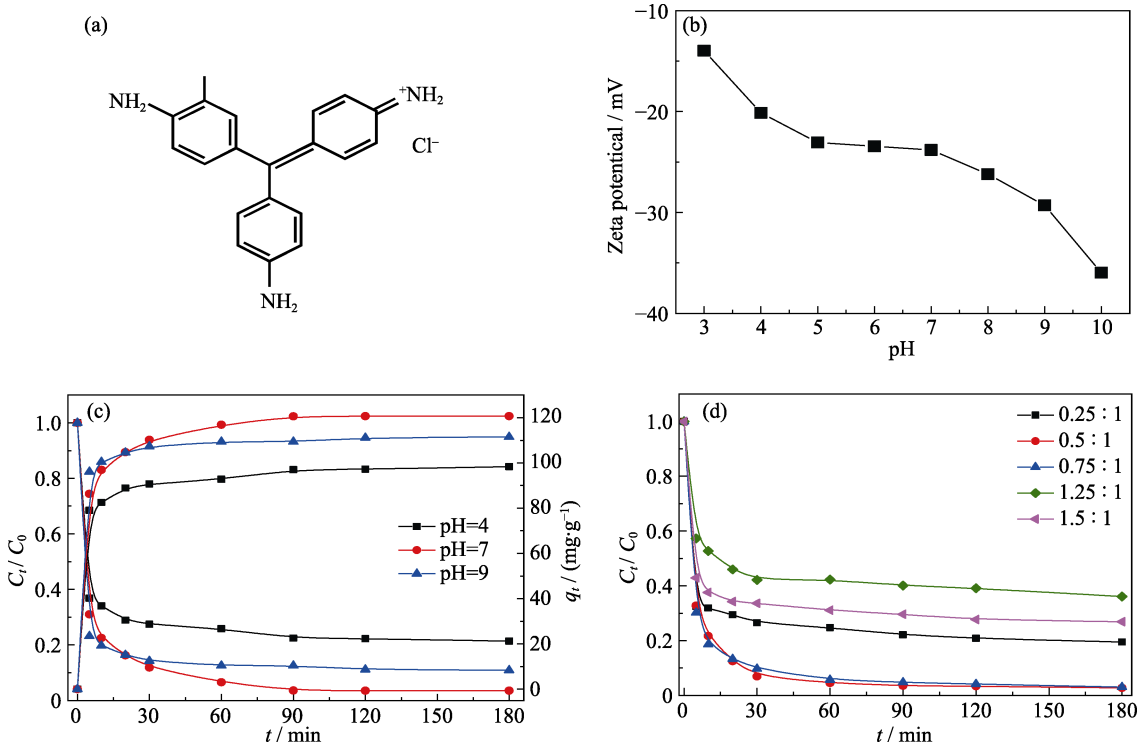

Fig. 7 Molecular structure of BF (a), Zeta potential of $Ni_3Si_2O_5(OH)_4$ microspheres (Ni/Si molar ratio of 1 : 1) (b), variation of the adsorption rate and capacity with adsorption time at different pH (Ni/Si molar ratio of 1 : 1) (c), and effect of Ni/Si molar ratio on the adsorption performance (d)

(Ni/Si molar ratio of 1∶1) (Fig. 7(c)). It shows that $Ni_3Si_2O_5(OH)_4$ possesses better adsorption property than $Ni_3Si_4O_{10}(OH)_2$. With the further increase of Ni/Si molar ratio to 1.25 and 1.5, the adsorption capacity was significantly decreased, which might be ascribed to the change in phase composition and the decrease of surface area as found by the XRD and BET measurement.

The adsorption kinetic for BF on $Ni_3Si_2O_5(OH)_4$ microspheres was also investigated. Two typical kinetic models, the pseudo-first-order (PFO) and pseudo-second-order (PSO) were applied to fit the adsorption data obtained from the time-dependent experiments. The linear fitting results are shown in Fig. S1, and the kinetic parameters as well as the determination coefficients (R^2) obtained by linear regression are listed in Table S2. The R^2 was as high as 0.9979, and meanwhile the calculated q_e (118.5 mg·g^{-1}) was very close to the experimental value (120.7 mg·g^{-1}), indicating that the PSO model was suitable to describe the adsorption kinetic of BF on $Ni_3Si_2O_5(OH)_4$ microspheres. Therefore, it can be considered a chemical adsorption process.

To give better insight into the removal efficiency of BF on $Ni_3Si_2O_5(OH)_4$ microspheres, comparison with the results in the literature using other adsorbents is made and the results are shown in Table S3. Various materials have been used as the adsorbents for the removal of BF from solution, including modified clay, molecular sieves, polymers, oxides/hydroxide, and many of them are composite materials. Table S3 reveals that $Ni_3Si_2O_5(OH)_4$ microspheres have a higher adsorption capacity than many adsorbents reported in recent years. Besides, they are also competitive in view of the simple preparation process. As comparison, $Ni_3Si_2O_5(OH)_4$ was also prepared by using SiO_2 templates according to the literature[19], and applied as adsorbent for BF removal. Under the same condition, its adsorption capacity was 101.0 mg·g^{-1}, less than that on the $Ni_3Si_2O_5(OH)_4$ microspheres in this study. As layered silicates, $Ni_3Si_2O_5(OH)_4$ microspheres have a much higher adsorption capacity than layered clay derived materials, such as alkali-activated diatomite, hydroxy-aluminum pillared bentonite, iron-manganese oxide coated kaolinite. A negative charge on the surface of the adsorbents is very beneficial for the adsorption of cationic dyes. And the pore structure and surface area also have significant effects on the adsorption capacity. In natural clays, the high negative charged framework is mainly balanced by alkali and alkali-earth cations, which limits the adsorption of cationic dyes. In hydroxy-aluminum pillared bentonite, the alkali and alkali-earth cations were replaced by inorganic hydroxy-metal polycations, bringing about lower surface potential and therefore contributing to the increase in adsorption capacity. $Ni_3Si_2O_5(OH)_4$ microspheres exhibited more negative Zeta potential comparing with hydroxy- aluminum pillared bentonite and iron-manganese oxide coated kaolinite, indicating a stronger charge-charge interaction with BF. Furthermore, the hierarchical porous structure of $Ni_3Si_2O_5(OH)_4$ microspheres rendered a much larger pore volume than hydroxy-aluminum pillared bentonite and alkali-activated diatomite.

The adsorption capacity of BF on $Ni_3Si_2O_5(OH)_4$ microspheres as function of the BF concentration in the solution at equilibrium conditions was investigated, and the Langmuir and Freundlich isotherm models were used to analyze the experimental data for the understanding of the adsorption mechanism. The experimental data of C_e and q_e are plotted in Fig. S2 and fitted according to the Langmuir and Freundlich isotherm models. The fitting parameters are listed in Table S4. As shown, when fitted with Freundlich model, the determination coefficient R^2 was 0.9919, much higher than that fitted with the Langmuir model(R^2 =0.7920), which revealed that the adsorption of BF on $Ni_3Si_2O_5(OH)_4$ microspheres was more consistent with the theory of multilayer adsorption. The $1/n$ value was 0.1678, indicating that the surface was heterogeneous[24] and the adsorption strength was strong.

3 Conclusions

When $NiCl_2$ and TEOS are used as the raw materials to prepare nickel phyllosilicate microspheres by the urea-assisted hydrothermal method, the Ni/Si molar ratio has a significant impact on the composition of the products. The suitable adding amount of TEOS is in excess of 50% than the stoichiometry of $Ni_3Si_2O_5(OH)_4$ to obtain pure-phase product. Compared with other alkali source, urea contributes to the assembly of the hierarchical porous microspheres because of the gradual release of OH^- ions and the CO_2 bubbles as soft-template. $Ni_3Si_2O_5(OH)_4$ microspheres have been proved to be an efficient adsorbent for removal of BF. The highly negative Zeta potential and the large pore volume are believed to be the significant factors for the strong adsorption strength and high adsorption capacity.

Suppporting Materials

Supporting materials related to this article can be found on the https://doi.org/10.15541/jim20210063.

References:

[1] RICHARD-PLOUET M, VILMINOT S, GUILLOT M. Synthetic transition metal phyllosilicates and organic-inorganic related

phases. *New Journal of Chemistry*, 2004, **28(9):** 1073–1082.
[2] MUNIRASU S, AGGARWAL R, BASKARAN D. Highly efficient recyclable hydrated-clay supported catalytic system for atom transfer radical polymerization. *Chemical Communications*, 2009**(30):** 4518–4520.
[3] SOETAREDJO F E, AYUCITRA A, ISMADJI S, *et al*. KOH/bentonite catalysts for transesterification of palm oil to biodiesel. *Applied Clay Science*, 2011, **53(2):** 341–346.
[4] BIAN Z, KAWI S. Preparation, characterization and catalytic application of phyllosilicate: a review. *Catalysis Today*, 2020, **339:** 3–23.
[5] HERNEY-RAMIREZ J, VICENTE MA, MADEIRA LM. Heterogeneous photo-Fenton oxidation with pillared clay-based catalysts for wastewater treatment: a review. *Applied Catalysis B: Environmental*, 2010, **98(1):** 10–26.
[6] KUMAR DUTTA D, JYOTI BORAH B, POLLOV SARMAH P. Recent advances in metal nanoparticles stabilization into nanopores of montmorillonite and their catalytic applications for fine chemicals synthesis. *Catalysis Reviews*, 2015, **57(3):** 257–305.
[7] JIANG B, LI L, BIAN Z, *et al*. Hydrogen generation from chemical looping reforming of glycerol by Ce-doped nickel phyllosilicate nanotube oxygen carriers. *Fuel*, 2018, **222:** 185–192.
[8] GHIAT I, BOUDJEMAA A, SAADI A, *et al*. Efficient hydrogen generation over a novel Ni phyllosilicate photocatalyst. *Journal of Photochemistry and Photobiology A: Chemistry*, 2019, **382:** 111952.
[9] LU Y, GUO D, ZHAO Y, *et al*. Confined high dispersion of Ni nanoparticles derived from nickel phyllosilicate structure in silicalite-2 shell for dry reforming of methane with enhanced performance. *Microporous and Mesoporous Materials*, 2021, **313:** 110842.
[10] KIM B, KIM JS, KIM H, *et al*. Amorphous multinary phyllosilicate catalysts for electrochemical water oxidation. *Journal of Materials Chemistry A*, 2019, **7(31):** 18380–18387.
[11] DI W, CHENG J, TIAN S, *et al*. Synthesis and characterization of supported copper phyllosilicate catalysts for acetic ester hydrogenation to ethanol. *Applied Catalysis A: General*, 2016, **510:** 244–259.
[12] BIAN Z, ZHONG W, YU Y, *et al*. Cu/SiO_2 derived from copper phyllosilicate for low-temperature water-gas shift reaction: role of Cu^+ sites. *International Journal of Hydrogen Energy*, 2020, **45(51):** 27078–27088.
[13] LEE Y C, KIM E J, YANG J W, *et al*. Removal of malachite green by adsorption and precipitation using aminopropyl functionalized magnesium phyllosilicate. *Journal of Hazardous Materials*, 2011, **192(1):** 62–70.
[14] SIVAIAH M V, PETIT S, BEAUFORT M F, *et al*. Nickel based catalysts derived from hydrothermally synthesized 1∶1 and 2∶1 phyllosilicates as precursors for carbon dioxide reforming of methane. *Microporous and Mesoporous Materials*, 2011, **140(1/2/3):** 69–80.
[15] MCDONALD A, SCOTT B, VILLEMURE G. Hydrothermal preparation of nanotubular particles of a 1∶1 nickel phyllosilicate. *Microporous and Mesoporous Materials*, 2009, **120(3):** 263–266.
[16] YANG Y, LIANG Q, LI J, *et al*. $Ni_3Si_2O_5(OH)_4$ multi-walled nanotubes with tunable magnetic properties and their application as anode materials for lithium batteries. *Nano Research*, 2011, **4(9):** 882–890.
[17] WHITE R D, BAVYKIN D V, WALSH F C. Morphological control of synthetic $Ni_3Si_2O_5(OH)_4$ nanotubes in an alkaline hydrothermal environment. *Journal of Materials Chemistry A*, 2013, **1(3):** 548–556.
[18] GUO Z, DU F, LI G, *et al*. Controlled synthesis of mesoporous $SiO_2/Ni_3Si_2O_5(OH)_4$ core-shell microspheres with tunable chamber structures *via* a self-template method. *Chemical Communications*, 2008**(25):** 2911–2913.
[19] CHEN D, GUO Z, SUN T, *et al*. Controlled synthesis and catalytic properties of mesoporous nickel-silica core-shell microspheres with tunable chamber structures. *Materials Research Bulletin*, 2012, **47(9):** 2344–2348.
[20] WANG T, LIU C, MA X, *et al*. Synthesis of $Ni_3Si_4O_{10}(OH)_2$ porous microspheres as support of Pd catalyst for hydrogenation reaction. *Nanomaterials*, 2019, **9(7):** 998.
[21] GROEN J C, PEFFER L A A, PÉREZ-RAMÍREZ J. Pore size determination in modified micro- and mesoporous materials. Pitfalls and limitations in gas adsorption data analysis. *Microporous and Mesoporous Materials*, 2003, **60(1/2/3):** 1–17.
[22] DONG F, XIONG T, WANG R, *et al*. Growth mechanism and photocatalytic activity of self-organized N-doped $(BiO)_2CO_3$ hierarchical nanosheet microspheres from bismuth citrate and urea. *Dalton Transactions*, 2014, **43(18):** 6631–6642.
[23] LI J, XU L, SUN P, *et al*. Novel application of red mud: facile hydrothermal-thermal conversion synthesis of hierarchical porous AlOOH and Al_2O_3 microspheres as adsorbents for dye removal. *Chemical Engineering Journal*, 2017, **321:** 622–634.
[24] MCKAY G, BLAIR H S, GARDNER J R. Adsorption of dyes on chitin. I. Equilibrium studies. *Journal of Applied Polymer Science*, 1982, **27(8):** 3043–3057.

多级多孔硅酸镍微球的合成及其对碱性品红的高效吸附

王婷婷, 史书梅, 柳晨媛, 朱万诚, 张 恒

(曲阜师范大学 化学与化工学院, 曲阜 273165)

摘 要: 层状硅酸镍因其独特的结构, 在电化学和催化等领域展现出良好的应用前景, 其合成与性能研究近年来受到广泛关注。本研究以氯化镍和正硅酸乙酯为原料, 采用水热法合成了硅酸镍微球, 并详细探究了镍硅比和碱源对产物组成、形貌及孔结构的影响。在优化条件下, 产物呈现由纳米片组装的、平均直径约为 2.5 μm 的微球形貌, 比表面积为 119.6 $m^2 \cdot g^{-1}$, 孔容为 0.673 $cm^3 \cdot g^{-1}$。Zeta 电位分析表明, 该微球在 pH=3~10 范围内保持表面电负性。将硅酸镍微球用于处理碱性品红溶液, 吸附过程符合准二级动力学模型。在初始浓度为 50 $mg \cdot L^{-1}$ 的条件下, 吸附容量可达 120.7 $mg \cdot g^{-1}$, 脱除率达 96.6%, 远优于改性粘土及近年来报道的多种材料。吸附量与平衡浓度的数据表明, 碱性品红在硅酸镍微球上的吸附符合 Freundlich 吸附模型, $1/n$=0.1678, 表明该吸附为多层非均相吸附且吸附作用力强。

关 键 词: 硅酸镍; 水热合成; 染料去除; 吸附; 碱性品红

中图分类号: TQ174 **文献标志码**: A

Supporting materials:

Synthesis of Hierarchical Porous Nickel Phyllosilicate Microspheres as Efficient Adsorbents for Removal of Basic Fuchsin

WANG Tingting, SHI Shumei, LIU Chenyuan, ZHU Wancheng, ZHANG Heng

(School of Chemistry and Chemical Engineering, Qufu Normal University, Qufu 273165, China)

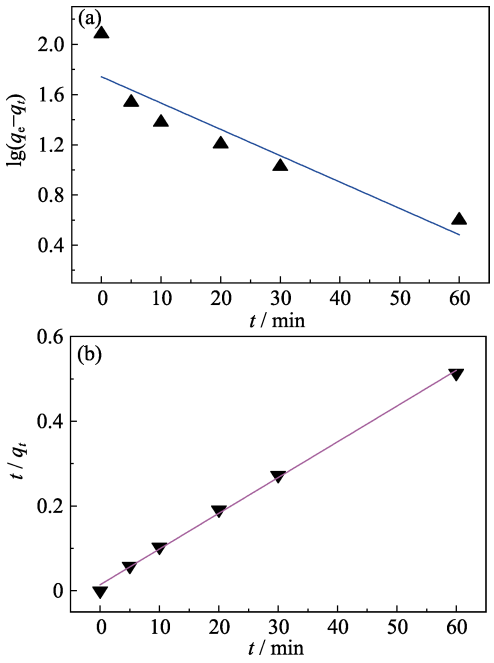

Fig. S1　Linear regression with pseudo-first-order (PFO) (a) and pseudo-second-order (PSO) (b) kinetic models

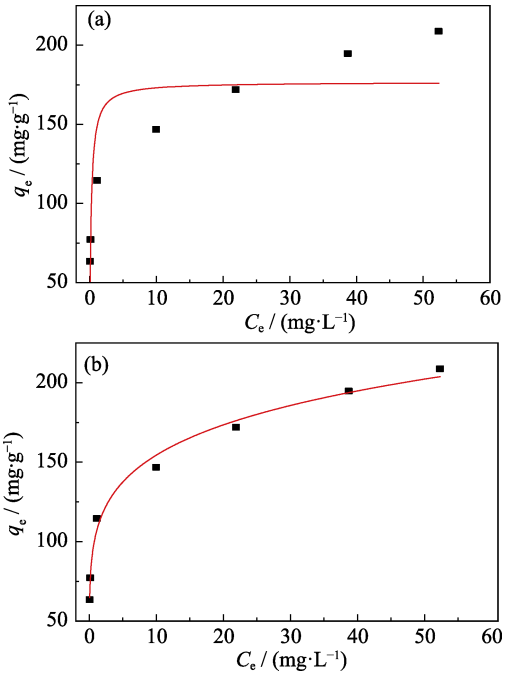

Fig. S2　Adsorption isotherms of BF on the $Ni_3Si_2O_5(OH)_4$ microspheres fitted with the Langmuir (a) and Freundlich (b) isotherm models

BF solution: 50 mg·L^{-1}, 50 mL; $Ni_3Si_2O_5(OH)_4$ microspheres (Ni/Si molar ratio of 1 : 1) : 20 mg. The linear regression equations for PFO and PSO models are expressed as Eqs. (1) and (2), respectively. In the equations, q_t (mg·g^{-1}) is the adsorption capacity at the corresponding time t (min) obtained from the experiments. And q_e (mg·g^{-1}), k_1 and k_2 (g·mg^{-1}·min^{-1}) are the fitting parameters, among which q_e refers to the calculated equilibrium adsorption capacity

$$\lg(q_e - q_t) = \lg q_e - \frac{k_1 t}{2.303} \quad \text{(S1)}$$

$$\frac{t}{q_t} = \frac{1}{k_2 q_e^2} - \frac{t}{q_e} \quad \text{(S2)}$$

The Langmuir and Freundlich isotherm models are expressed as Eqs. (3) and (4), respectively. In the equations, C_e (mg·L^{-1}) and q_e (mg·g^{-1}) are the concentration of the adsorbate in solution and its amount on the adsorbent at equilibrium, respectively. For Langmuir isotherm model, q_m (mg·g^{-1}) is the theoretical maximum adsorption capacity corresponding to entire monolayer adsorption, and b (L·mg^{-1}) is the equilibrium constant connected with the energy of adsorption. For Freundlich isotherm model, which indicates the nonideal multilayer adsorption on active sites with nonuniform distribution of adsorption heat and affinities throughout the heterogeneous surface, K_f and $1/n$ are the isotherm constants, representing the adsorption capacity at unit concentration and the adsorption strength, respectively.

$$q_e = \frac{q_m b C_e}{1 + b C_e} \quad \text{(S3)}$$

$$q_e = K_f C_e^{1/n} \quad \text{(S4)}$$

Table S1　Textural properties of the products

Ni/Si molar ratio	S_{BET} /(m^2·g^{-1})	Pore volume /(cm^3·g^{-1})	Average pore diameter/nm
0.5 : 1	139.4	0.884	6.00
0.75 : 1	128.2	0.511	5.58
1 : 1	119.6	0.673	5.90
1.25 : 1	101.1	0.426	5.86
1.5 : 1	95.5	0.564	8.68

Table S2 Adsorption kinetic model parameters for the adsorption of BF on the $Ni_3Si_2O_5(OH)_4$ microspheres

$q_{e,exp}$ /(mg·g^{-1})	Pseudo-first-order kinetic model			Pseudo-second-order kinetic model		
	$q_{e,calc1}$/(mg·g^{-1})	k_1/min^{-1}	R^2	$q_{e,calc2}$/(mg·g^{-1})	k_2/(mg·g^{-1}·min^{-1})	R^2
120.7	55.2	0.0483	0.8526	118.5	0.0051	0.9979

Table S3 Comparison of the adsorption capacities for BF on various adsorbents

Adsorbents	Initial concentration of BF solution/(mg·L^{-1})	Adsorption equilibrium time/min	Maximum adsorption capacity /(mg·g^{-1})	Ref.
Alkali-activated diatomite	15	30	4.85	[1]
(Acrylamide-co-sodium methacrylate)-*graft*-chitosan gel	125	180	6.1	[2]
β-cyclodextrin-carboxymethyl cellulose-graphene oxide composite	100	150	6.5	[3]
Hydroxy-aluminum pillared bentonite	100	10–15	6.6	[4]
Iron-manganese oxide coated kaolinite	40	50	8.16	[5]
Copper vinylphosphonate	30	150	19.29	[6]
Fe-ZSM-5	20	240	25.8	[7]
β-cyclodextrin-styrene-based polymer	50	180	29.6	[8]
$CoFe_2O_4$-HA-ECH	33.8	30	31.3	[9]
Magnetic chitosan/graphene oxide	50	70	32.8	[10]
Activated carbon/ferrospinel composite	100	60	49.9	[11]
Al-MCM-41	60	240	54	[12]
$Ba(B_2Si_2O_8)$ microspheres	30	240	58.0	[13]
$NiFe_2O_4$/polythiophene nanocomposite	50	30	76	[14]
$Ni_3Si_2O_5(OH)_4$	50	180	120.7	This work

Table S4 Corresponding fitting parameters originated from the non-linear regression by using Langmuir and Freundlich isotherm models

Langmuir isotherm model			Freundlich isotherm model		
q_m/(mg·g^{-1})	b/(L·mg^{-1})	R^2	k_f	1/n	R^2
176.7	4.7474	0.7920	104.9	0.1678	0.9919

References:

[1] ZHAO YH, GENG JT, CAI JC, *et al*. Adsorption performance of basic fuchsin on alkali-activated diatomite. *Adsorption Science & Technology*, 2020, **38(5/6):** 151–167.

[2] IBRAHIM A G, SAYED A Z, ABD EL-WAHAB H, *et al*. Synthesis of a hydrogel by grafting of acrylamide-co-sodium methacrylate onto chitosan for effective adsorption of Fuchsin basic dye. *International Journal of Biological Macromolecules*, 2020, **159:** 422–432.

[3] YUAN J, QIU F, LI P. Synthesis and characterization of β-cyclodextrin-carboxymethyl cellulose-graphene oxide composite materials and its application for removal of basic fuchsin. *Journal of the Iranian Chemical Society*, 2017, **14(9):** 1827–1837.

[4] HAO Y, YAN L, YU H, *et al*. Comparative study on adsorption of basic and acid dyes by hydroxy-aluminum pillared bentonite. *Journal of Molecular Liquids*, 2014, **199:** 202–207.

[5] KHAN T A, KHAN E A, SHAHJAHAN. Removal of basic dyes from aqueous solution by adsorption onto binary iron-manganese oxide coated kaolinite: non-linear isotherm and kinetics modeling. *Applied Clay Science*, 2015, **107:** 70–77.

[6] NISTOR M A, MUNTEAN S G, MARANESCU B, *et al*. Phosphonate metal-organic frameworks used as dye removal materials from wastewaters. *Applied Organometallic Chemistry*, 2020, **34(11):** e5939.

[7] BA MOHAMMED B, HSINI A, ABDELLAOUI Y, *et al*. Fe-ZSM-5 zeolite for efficient removal of basic Fuchsin dye from aqueous solutions: synthesis, characterization and adsorption process optimization using BBD-RSM modeling. *Journal of Environmental Chemical Engineering*, 2020, **8(5):** 104419.

[8] LI X, XIE L, YANG X, *et al*. Adsorption behavior and mechanism of *β*-cyclodextrin-styrene-based polymer for cationic dyes. *RSC Advances*, 2018, **8(70):** 40321–40329.

[9] SAKTI S C W, LAILY R N, ALIYAH S, *et al*. Re-collectable and recyclable epichlorohydrin-crosslinked humic acid with spinel cobalt ferrite core for simple magnetic removal of cationic triarylmethane dyes in polluted water. *Journal of Environmental Chemical Engineering*, 2020, **8(4):** 104004.

[10] LI L, FAN L, LUO C, *et al*. Study of fuchsine adsorption on magnetic chitosan/graphene oxide. *RSC Advances*, 2014, **4(47):** 24679–24685.

[11] AI L, JIANG J. Fast removal of organic dyes from aqueous solutions by AC/ferrospinel composite. *Desalination*, 2010, **262(1):** 134–140.

[12] GUAN Y, WANG S, WANG X, *et al*. Preparation of mesoporous Al-MCM-41 from natural palygorskite and its adsorption performance for hazardous aniline dye-basic fuchsin. *Microporous and Mesoporous Materials*, 2018, **265:** 266–274.

[13] MIAO J, ZHAO X, LI Y, *et al*. Facial preparation of hierarchical porous $Ba(B_2Si_2O_8)$ microsphere by sacrificial-template method and its highly efficient selective adsorption of triphenylmethane dyes. *Colloids and Surfaces A*, 2020, **602:** 124883.

[14] HUSSAIN D, SIDDIQUI M F, KHAN T A. Preparation of $NiFe_2O_4$/polythiophene nanocomposite and its enhanced adsorptive uptake of Janus green B and Fuchsin basic from aqueous solution: Isotherm and kinetics studies. *Environmental Progress & Sustainable Energy*, 2020, **39(3):** e13371.